Parameter Optimization of Spread Spectrum Modulation to Minimize EMI Filter for Interleaved Totem-Pole PFC Converters

Jiho Song[1], Chang-Yeob Chu[1], Youngseok Lee[1], Dong-In Lee[2], Han-Shin Youn[2], and Ki-Bum Park[1]
[1] Cho Chun Shik Graduate School of Mobility, Korea Advanced Institute of Science and Technology, Korea
[2] Department of Electrical Engineering, Incheon National University, Korea

***Abstract*—Recently, with SiC devices, switching frequency and electromagnetic interference (EMI) noise are increasing for power factor correction (PFC) converters, and EMI filter is used to reduce EMI noise. However, when EMI filter size is reduced from 2-stage and 1-stage for increasing power density, there is a problem that EMI noise is increasing and EMI standard is no longer satisfied with conventional fixed frequency modulation (FFM). To solve this problem, parameter optimization of spread spectrum modulation (SSM) is performed in this paper. Considering waveform shape, amplitude, and frequency of switching frequency, an optimal switching frequency for minimizing EMI noise is found. As a result, EMI noise is minimized when waveform shape is random and amplitude is 18 kHz, and EMI margin is 11.13 %. Therefore, it is possible to reduce EMI filter size with optimized SSM, and also there is no difference in terms of inductor and switch losses.**

***Index Terms*—Electromagnetic interference (EMI), EMI filter reduction, power factor correction (PFC), spread spectrum modulation (SSM).**

I. Introduction

Recently, with development of SiC devices, switching frequency and electromagnetic interference (EMI) noise tend to be increased for power factor correction (PFC) converters. Fig. 1 shows schematic of an interleaved totem-pole PFC converter, which has lower system loss and input current ripple. As shown Fig. 1, an EMI filter including X-capacitor, Y-capacitor, and common-mode (CM) choke inductor is used for reducing EMI noise. Due to heavy and bulky passive components, it is important to reduce EMI filter size for increasing power density.

However, when EMI filter size is reduced from 2-stage to 1-stage shown as Fig. 1, EMI noise is increasing and then EMI standard for vehicles, CISPR 25 [1], is no longer satisfied with conventional fixed frequency modulation (FFM) shown as Fig. 2. It leads to a problem for reducing EMI noise.

To solve this problem without any additional hardware, some studies using spread spectrum modulation (SSM) have been performed for boost PFC converter [2]-[4], 3-level boost PFC converter [5], flyback PFC converter [6], and interleaved bridgeless PFC converter [7]. SSM is a modulation method using time-varying switching frequency with specific pattern, which makes EMI noise at specific frequency distributed around specific frequency band shown as Fig. 2.

The limitation of these studies is that various SSM parameters including waveform shape, amplitude, and frequency of switching frequency are not considered for minimizing EMI noise. Especially, for waveform shape, specific waveform shapes are used such as triangle waveform [2], [4], [5], sawtooth waveform [6], random waveform [3], and cosine waveform [7].

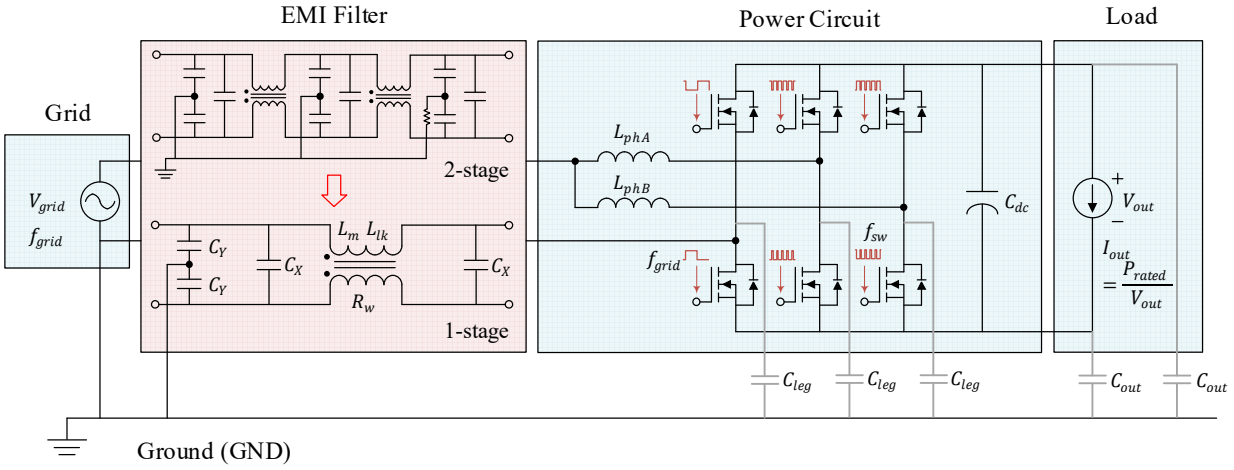

Fig. 1. Schematic of interleaved totem-pole PFC converter with an EMI filter reduced from 2-stage to 1-stage.

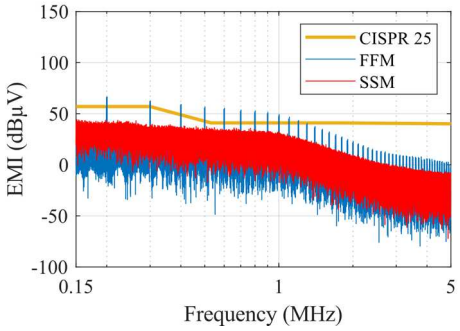

Fig. 2. Comparison of EMI spectrum between modulation methods: Conventional FFM vs. SSM.

To differentiate from previous works, SSM parameter optimization for minimizing EMI noise considering various SSM parameters is performed in this paper. Triangle, sine, rectangle, and random waveform are considered as SSM parameters. After simulation using PSIM, optimal switching frequency for minimizing EMI noise is found with the highest EMI margin, which means minimum difference between measured EMI value and EMI standard at specific frequency. Also, loss analysis is performed whether there are disadvantages in terms of inductor and switch losses. As a result, this study provides a simulation-based verification that EMI filter can be reduced from 2-stage to 1-stage with optimized SSM.

II. Spread Spectrum Modulation

A. Interleaved totem-pole PFC converter

Fig. 3 shows system overview and control structure of interleaved totem-pole PFC converter [8]-[9]. The system operates by measuring grid voltage V_{grid}, inductor currents iL_{phA}, iL_{phB}, and output voltage V_{out}, and generating duty D. The duty is compared with phase A and B carriers with 180 degrees phase shift angle, and gate signals G_{sw} for switching operation are generated.

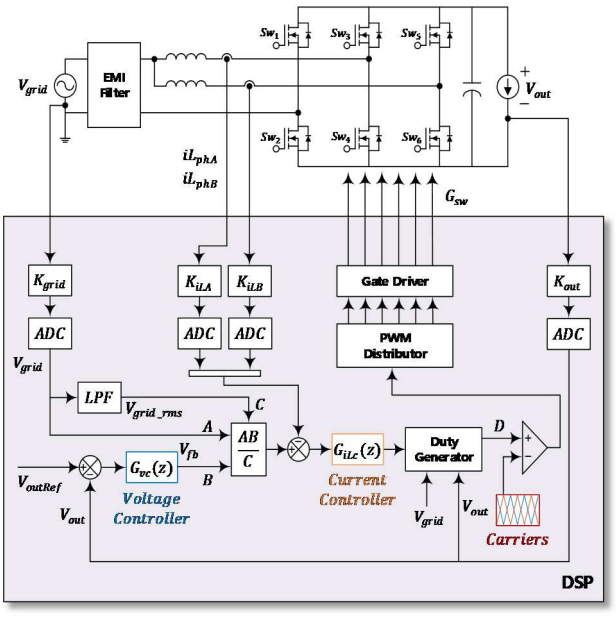

Fig. 3. System overview and control structure of interleaved totem-pole PFC converter.

Fig. 4 shows comparison of waveform of the carriers used for control between FFM and SSM. Unlike FFM using carriers with constant period in Fig. 4(a), SSM focuses on using carriers with time-varying period shown in Fig. 4(b).

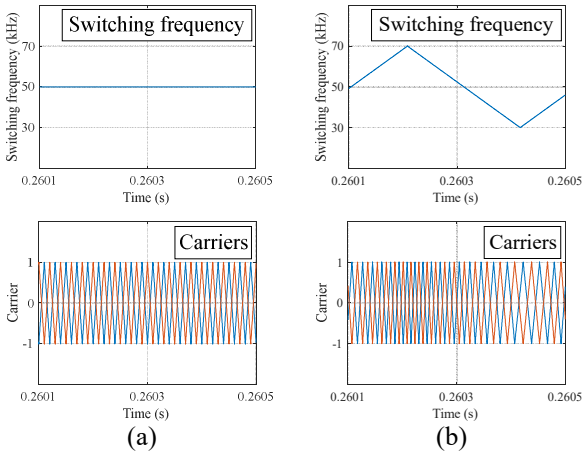

Fig. 4. Comparison of waveform of the carriers for control between (a) FFM and (b) SSM.

B. Conducted EMI noise

Due to switching operation of the converter, EMI noise is generated. EMI noise is classified as conducted EMI noise moving through electric line or ground with 150kHz~30MHz, and radiated EMI noise moving through air with more than 30MHz.

The conducted EMI noise, interested in this paper, is classified as common-mode (CM) noise and differential-mode (DM) noise according to noise path. CM noise is moving to grid through ground, where CM noise source is connected to parasitic capacitor existing between chassis and converter shown as Fig. 5(a). Meanwhile, DM noise is moving to grid through power lines, where DM noise source is connected to converter and power lines in Fig. 5(b).

C. Impact of SSM on EMI noise

SSM can be used for reducing these EMI noises. In this paper, SSM is implemented by updating to new switching frequency, switching period, maximum of count, and carrier waveform whenever count becomes zero [10]. Fig. 6 shows implementation of SSM in detail. The count is incremented or decremented by one per sampling period. The count is increasing until the count becomes maximum of count, and decreasing until the count becomes zero. Whenever count becomes zero, switching frequency $f_{sw}[k]$ and switching period $T_{sw}[k]$ are updated to new value $f_{sw}[k+1]$, $T_{sw}[k+1]$, and maximum of count corresponding to the updated switching period $Cnt_{max}[k+1]$ is calculated, and the new count waveform is generated. Eventually, carrier waveform with time-varying period is generated based on count and maximum of count. By using SSM, EMI noise source is spread over a certain frequency range shown as Fig. 7, and finally EMI noise is reduced. On the other hand, EMI filter is reducing EMI noise already generated. It is major difference between SSM and EMI filter.

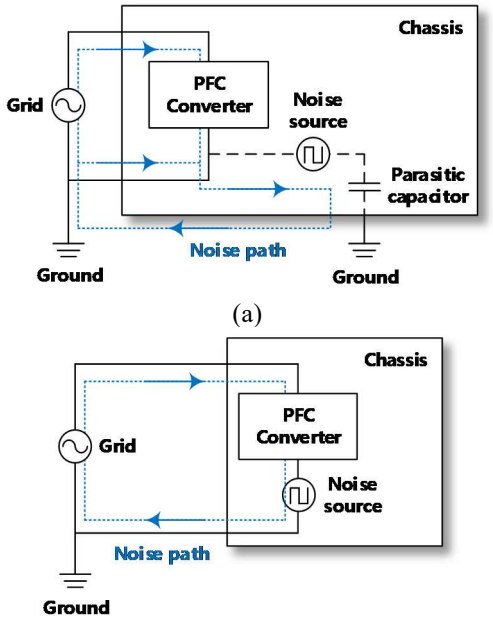

Fig. 5. Two kinds of conducted EMI noises. (a) CM noise. (b) DM noise.

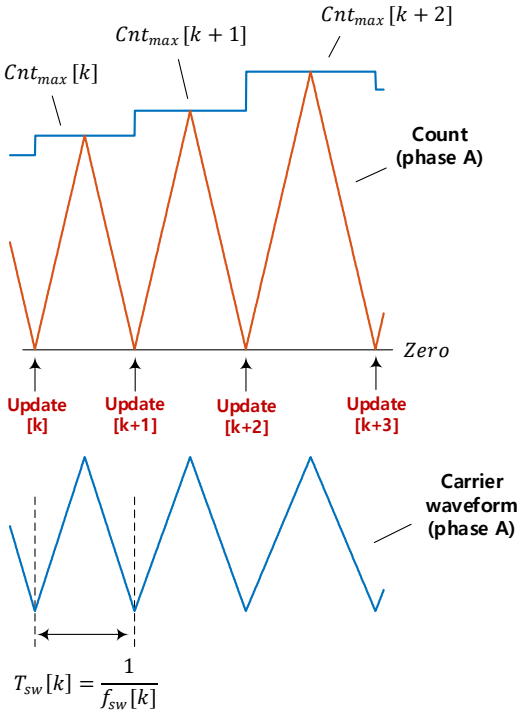

Fig. 6. Implementation of SSM.

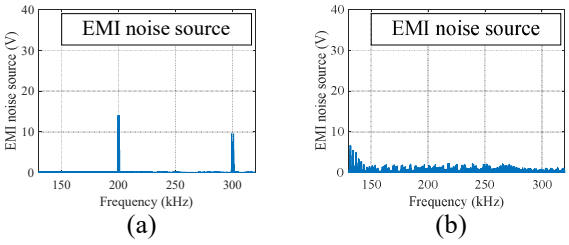

Fig. 7. Comparison of EMI noise source between (a) FFM and (b) SSM.

D. SSM parameters

To implement SSM, waveform of switching frequency is most important. SSM parameters for determining waveform of switching frequency include waveform shape, amplitude, and frequency.

Fig. 8 shows impacts of SSM parameters on carrier waveforms and EMI spectrums. In this paper, rectangle, sine, triangle, and uniform distributed random wave are considered as waveform shapes. When the switching frequency changes with certain amplitude, the density of carrier wave increases when switching frequency is higher than base switching frequency, 50 kHz in this paper, and on the other hand, the density of carrier wave decreases when switching frequency is lower than base switching frequency.

Fig. 8(a) shows comparison of carrier waveforms and EMI spectrums among waveform shapes of switching frequency. For rectangle wave, due to drastic change of switching frequency, increase and decrease in density of carrier wave are clear. It leads to irregular increase of EMI noise. For sine and triangle waves, carrier waves look similar, but there is a difference in density of carrier wave nearby maximum or minimum of switching frequency. It is because switching frequency of sine wave maintains a higher or lower value than that of triangle wave during the same time. Therefore, EMI noise of triangle wave is flatter than that of sine wave. For random wave, carrier wave changes randomly, so reduction of EMI noise for random wave is best among other waveform shapes.

Fig. 8(b) shows carrier waveforms and EMI spectrums according to amplitude of switching frequency. Value of amplitude means how far away from the base switching frequency it changes. The amplitude from 2 kHz to 20 kHz are considered in this paper. The maximum limit is determined by transfer function of EMI filter, and it will be discussed in next section. As the amplitude is increasing, increase and decrease in density of carrier wave appear more distinctly. Also, EMI noise spectrum tends to be flatter for triangle wave according to increase of amplitude.

Fig. 8(c) shows carrier waveforms and EMI spectrums according to frequency of switching frequency. The frequency from 0.24 kHz to 2.4 kHz are considered in this paper. As the frequency is increasing, high and low density of carrier waveform appear more frequently. However, EMI spectrum tends to increase slightly for triangle wave according to increase of frequency.

The results in Fig. 8 are made by performing EMI simulation using PSIM. The system specification and sweep range of SSM parameters are shown in Table I and Table II, respectively. In this paper, a time-domain simulation-based study is conducted due to nonlinear characteristic of EMI analyzer for quasi-peak detection.

In terms of EMI spectrum, Fig. 8(b) and Fig. 8(c) show results for only triangle wave. Therefore, it is required to analyze EMI noise considering aforementioned SSM parameters and optimize SSM parameters for minimizing EMI noise and EMI filter.

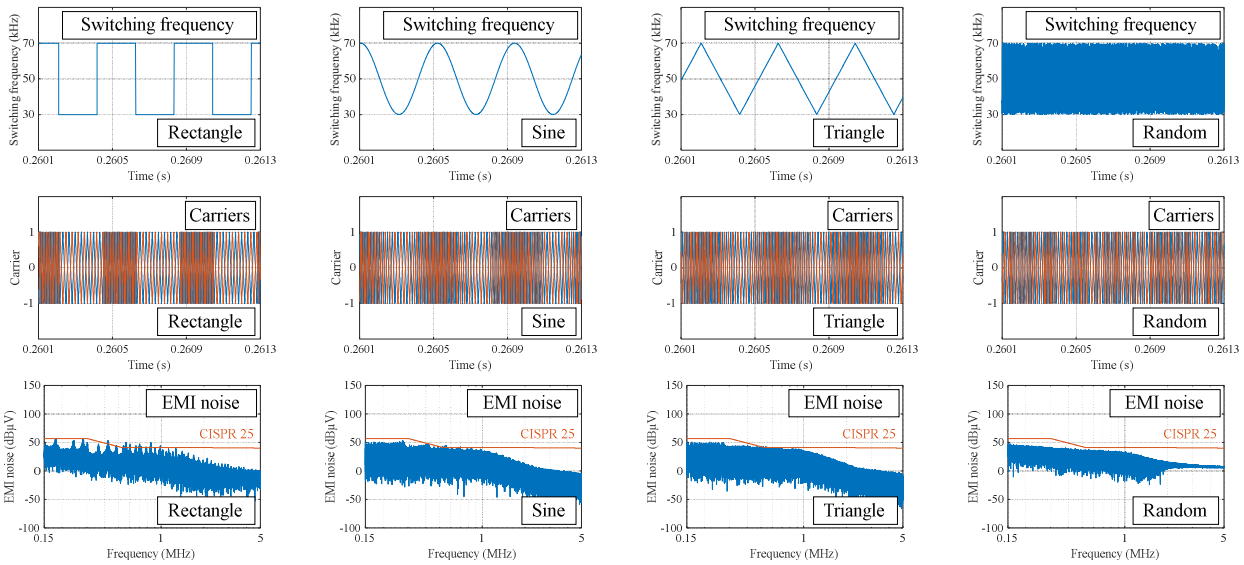

(a)

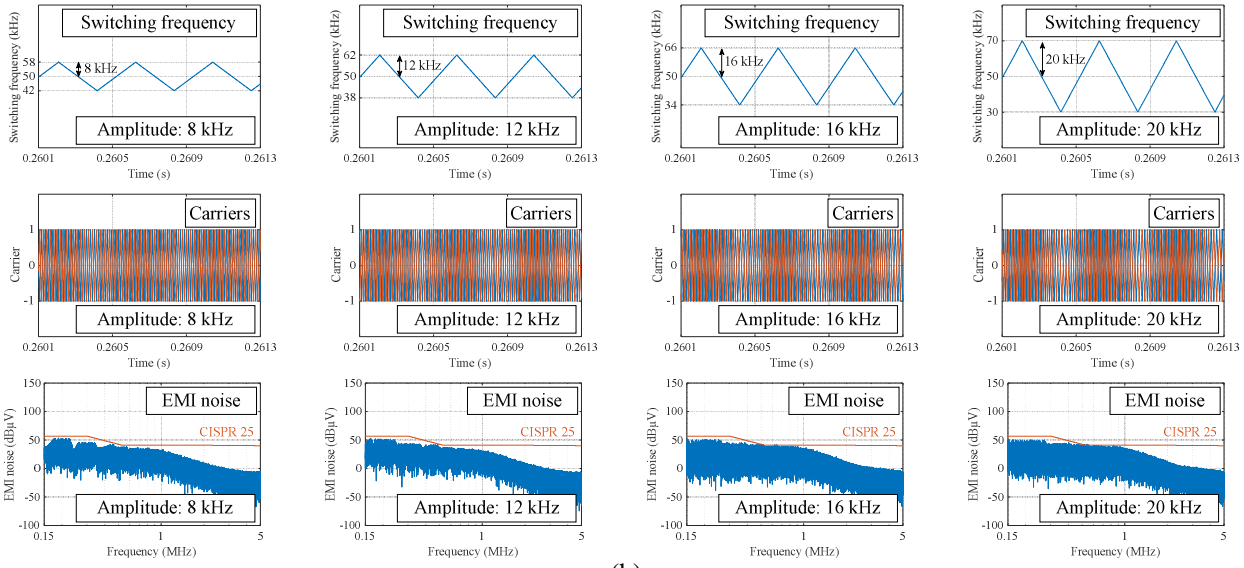

(b)

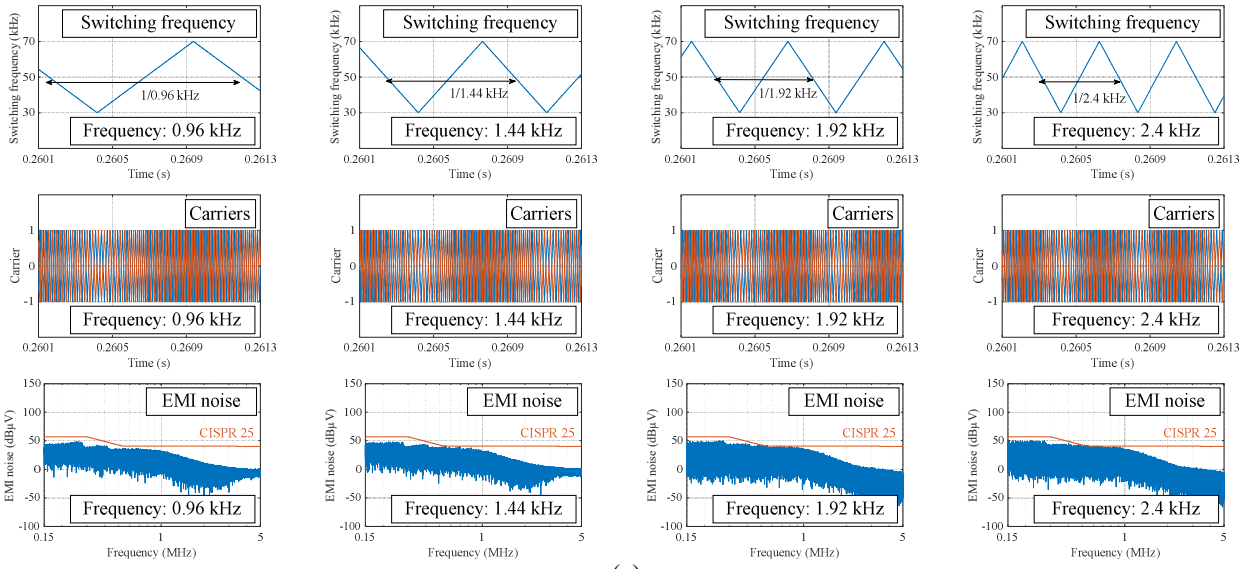

(c)

Fig. 8. Carrier waveforms and EMI spectrums according to SSM parameters. (a) Waveform shape. (b) Amplitude. (c) Frequency.

TABLE I
SYSTEM SPECIFICATION

Variable			Symbol	Value
Grid voltage			V_{grid}	220 V_{rms}
Grid frequency			f_{grid}	60 Hz
Output voltage			V_{out}	400 V
DC-link capacitance			C_{dc}	660 µF
Inductance of boost inductor			L_{phA}, L_{phB}	744 µH
Rated power			P_{rated}	3.3 kW
100% load current			I_{out}	8.25 A
Base switching frequency			$f_{sw(base)}$	50 kHz
Parasitic capacitance		Output terminal to ground	C_{out}	250 pF
		Each switch leg to ground	C_{leg}	45 pF
EMI filter	X-capacitor	Capacitance	C_X	2.2 µF
	Y-capacitor	Capacitance	C_Y	4.7 nF
	CM chock inductor	Magnetizing inductance	L_m	3.7 mH
		Leakage inductance	L_{lk}	3.5 µH
		Winding resistance	R_w	5 mΩ

TABLE II
SWEEP RANGE OF SSM PARAMETERS

SSM Parameters	Value
Waveform shape	Rectangle, Sine, Triangle, Random
Amplitude	2, 4, …, 18, 20 kHz (4% ~ 40% of $f_{sw(base)}$)
Frequency	0.24, 0.48, …,1.92, 2.4 kHz (4 ~ 40 times f_{grid})

III. PARAMETER OPTIMIZATION OF SSM

A. Amplitude limit

The Amplitude of switching frequency is limited by transfer function of EMI filter as previously mentioned. Fig. 9 shows schematic of EMI filter and equivalent circuit of CM and DM filter when EMI filter size is reduced from 2-stage to 1-stage. Fig. 10 shows transfer function of the CM and DM filter. It is important to know at what switching frequency the resonance occurs for CM and DM filter. It is because EMI noise can increase due to the resonance. From Fig. 10, CM and DM filter have resonance points at 30 kHz and 40 kHz, respectively. For avoiding resonance points, range of switching frequency of 30 kHz to 70 kHz is considered in this paper. The range is reasonable because frequency of EMI noise is twice the switching frequency due to interleaving operation.

B. EMI margin

For quantitative analysis, EMI margin is defined as EMI performance index in this paper. EMI margin means minimum of EMI difference ($\Delta\, EMI$) between measured EMI ($EMI_{measured}$) and EMI standard ($EMI_{standard}$) shown as Fig. 11. EMI margin is calculated by (1) and (2). When EMI margin < 0, it means measured EMI is higher than EMI standard. On the other hand, when EMI margin > 0, it means measured EMI is lower than EMI standard. Also, a larger EMI margin means more margin from the EMI standard and less measured EMI. Therefore, in this paper, the objective is to perform parameter optimization for maximizing the EMI margin.

$$\Delta\, EMI = \frac{EMI_{standard} - EMI_{measured}}{EMI_{standard}} \times 100\ (\%) \quad (1)$$

$$EMI\ margin = \min(\Delta\, EMI) \quad (2)$$

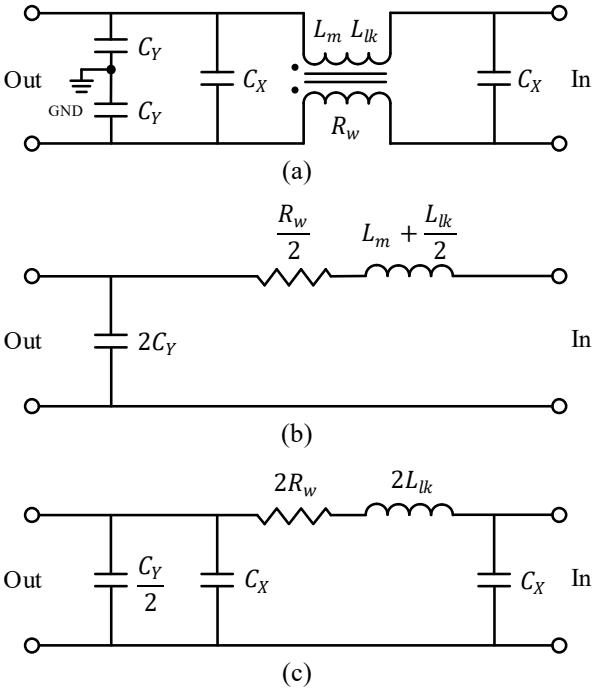

Fig. 9. (a) Schematic of EMI filter and equivalent circuit of (b) CM filter and (c) DM filter.

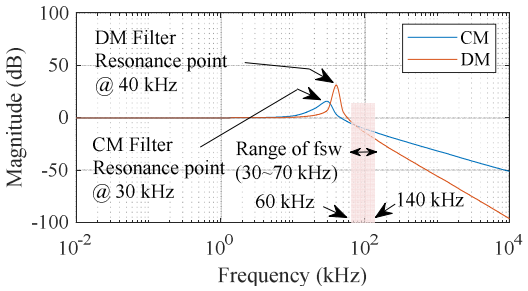

Fig. 10. Transfer function of CM and DM filter.

C. Parameter optimization

Considering SSM parameters shown Table II, the parameter optimization results for minimizing EMI noise are shown as Fig. 12. X-axis is the amplitude of switching frequency in kHz, and y-axis is the EMI margin in %. The red, green, black, and blue lines are the EMI margin for random, triangle, sine, and rectangle waves, respectively. For periodic waves such as triangle, sine, and rectangle

waves, ten lines corresponding to the sweep range of frequency of switching frequency is shown in Fig. 12. The random wave is independent of the frequency, so there is a line for random wave in Fig. 12. Rectangle waves (blue lines) show the lowest EMI margin, and triangle waves (green lines) are superior to sine waves (black lines) in some cases. Random wave (a red line) has higher EMI margin than other periodic waves in most cases. As a result of the parameter optimization, the optimal point with highest EMI margin occurs when waveform shape is random wave, and amplitude of switching frequency is 18 kHz. And then EMI margin is 11.13 %.

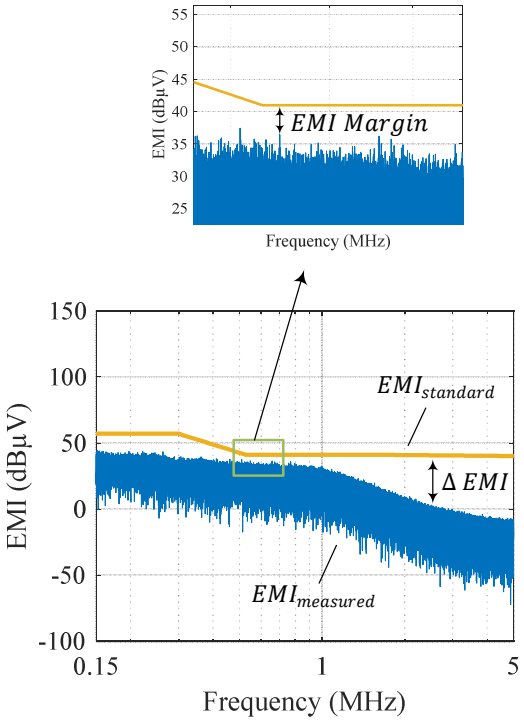

Fig. 11. Calculation of EMI margin.

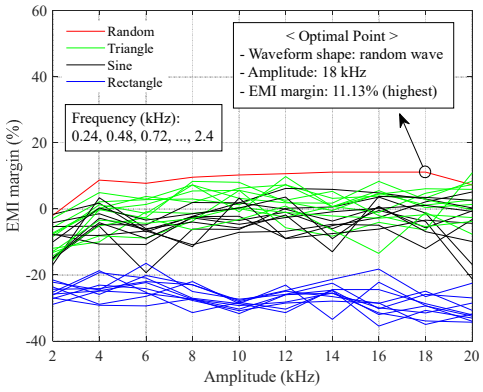

Fig. 12. SSM parameter optimization results.

Fig. 13 shows comparison of EMI filter size between FFM with 2-stage EMI filter, and optimized SSM with 1-stage EMI filter. For FFM, 2-stage EMI filter is required to satisfy EMI standard, CISPR 25 shown as Fig. 13(a). Otherwise, a problem about dissatisfaction to EMI standard occurs as discussed introduction (Fig. 2). However, the EMI filter size can be reduced from 2-stage to 1-stage using the parameter optimized SSM discussed in this paper shown as Fig. 13(b). Therefore, it is verified that EMI filter size reduction is enable by using SSM.

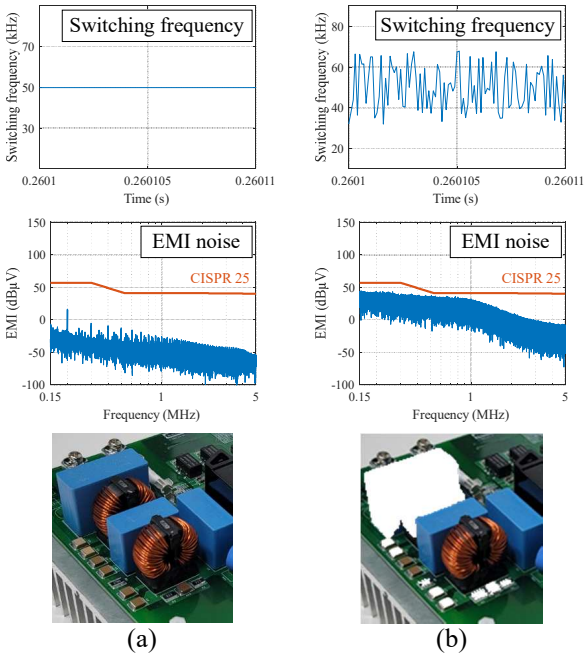

Fig. 13. Comparison of EMI filter size:
(a) FFM with 2-stage EMI filter.
(b) optimized SSM with 1-stage EMI filter.

D. Loss analysis

Fig. 14(a) shows comparison of inductor and switch losses between FFM and SSM at full load. Most losses occur in switches. Total losses including boost inductor loss and switch loss are 48.16 W for FFM, and 47.36 W for SSM. As a result, the difference between two total losses is by only about 0.8 W. It means that with SSM, there is little difference in loss. Fig. 14(b) shows comparison of the inductor and switch losses between FFM and SSM according to load. 100% load means full load shown as Fig. 14(a). It is noted that there is no difference between losses of FFM and SSM despite change of modulation.

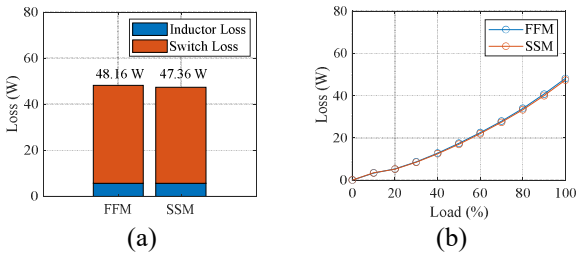

Fig. 14. Comparison of boost inductor and switch losses between FFM and SSM
(a) at full load and (b) according to load.

IV. Conclusions

In this paper, parameter optimization for minimizing EMI filter size is performed. When waveform shape of switching frequency is random wave, and amplitude of

switching frequency is 18 kHz, optimal point to minimize EMI noise occurs. And then EMI margin is 11.13 %. With the parameter optimized SSM, it is verified that EMI filter can be reduced from 2-stage to 1-stage. So, power density can be increasing and cost can be reduced. In loss analysis, total losses including boost inductor loss and switch loss are found to be nearly the same value between conventional FFM and parameter optimized SSM. Therefore, existing cooling system can be used, and there can be no additional cost.

For further works, related experiments including EMI measurement setup such as LISN and EMI analyzer will be performed to verify reduction of EMI filter size using SSM.

ACKNOWLEDGMENT

This research was supported by UNDERGROUND CITY OF THE FUTURE program funded by the Ministry of Science and ICT.

REFERENCES

[1] *Vehicles, boats and internal combustion engines – Radio disturbance characteristics – Limits and methods of measurement for the protection of on-board receivers*, CISPR 25, CISPR, p. 54, 2021.

[2] J. -C. Le Bunetel, D. Gonzalez and J. Balcell, "Impact of Periodic Switching Frequency Modulation control to reduce conducted EMI in Power Factor Converters," *IECON 2006 - 32nd Annual Conference on IEEE Industrial Electronics*, Paris, France, 2006, pp. 2541-2545.

[3] Y. -S. Lai and K. -M. Ho, "Novel random switching PWM with constant sampling frequency and constant inductor average current for digital-controlled power factor corrector," *2012 IEEE Energy Conversion Congress and Exposition (ECCE)*, Raleigh, NC, USA, 2012, pp. 4577-4583.

[4] N. Oiwa et al., "EMI Noise Reduction for PFC Converter with Improved Efficiency and High Frequency Clock," *2018 14th IEEE International Conference on Solid-State and Integrated Circuit Technology (ICSICT)*, Qingdao, China, 2018, pp. 1-3.

[5] M. Lee and J. -S. Lai, "Spread-Spectrum Frequency Modulation With Adaptive Three-Level Current Scheme to Improve EMI and Efficiency of Three-Level Boost DCM PFC," *IEEE Transactions on Power Electronics*, vol. 36, no. 3, pp. 2476-2480, March 2021.

[6] D. Stepins, "An Improved Control Technique of Switching-Frequency-Modulated Power Factor Correctors for Low THD and High Power Factor," *IEEE Transactions Power Electronics*, vol. 31, no. 7, pp. 5201-5214, July 2016.

[7] Q. Li, O. C. Thomsen and M. A. E. Andersen, "Research on EMI reduction of interleaved Bridgeless Power Factor Corrector using frequency dithering," *Proceedings of The 7th International Power Electronics and Motion Control Conference*, Harbin, China, 2012, pp. 1065-1069.

[8] Y. Tang, W. Ding and A. Khaligh, "A bridgeless totem-pole interleaved PFC converter for plug-in electric vehicles," *2016 IEEE Applied Power Electronics Conference and Exposition (APEC)*, Long Beach, CA, USA, 2016, pp. 440-445.

[9] H. -S. Youn, J. -S. Park, K. -B. Park, J. -I. Baek and G. -W. Moon, "A Digital Predictive Peak Current Control for Power Factor Correction With Low-Input Current Distortion," *IEEE Transactions Power Electronics*, vol. 31, no. 1, pp. 900-912, Jan. 2016.

[10] K. -B. Park, P. Klaus and R. M. Burkart, "Spread Spectrum Modulation for LCL Filter Design," *2019 20th International Symposium on Power Electronics (Ee)*, Novi Sad, Serbia, 2019, pp. 1-6.